

Learning to Segment Liquids in Real-world Images

Jonas Li Michelle Li Luke Liu Heng Fan
University of North Texas

Abstract

Different types of liquids such as water, wine and medicine appear in all aspects of daily life. However, limited attention has been given to the task, hindering the ability of robots to avoid or interact with liquids safely. The segmentation of liquids is difficult because liquids come in diverse appearances and shapes; moreover, they can be both transparent or reflective, taking on arbitrary objects and scenes from the background or surroundings. To take on this challenge, we construct a large-scale dataset of liquids named LQDS consisting of 5000 real-world images annotated into 14 distinct classes, and design a novel liquid detection model named LQDM, which leverages cross-attention between a dedicated boundary branch and the main segmentation branch to enhance segmentation predictions. Extensive experiments demonstrate the effectiveness of LQDM on the test set of LQDS, outperforming state-of-the-art methods and establishing a strong baseline for the semantic segmentation of liquids. Our benchmark and code will be released at: <https://lonaslee.github.io/LQDM>.

1. Introduction

Liquids are everywhere in the real world, such as in household kitchens, restaurants, and in nature. As a result of this frequency, the task of segmenting them is important and widely applicable. For instance, a robot may need to distinguish between different types of drinks to fulfill a user request. Additionally, when traversing a factory or nature, a robot must recognize spills or ponds to plan its path around them.

Liquids present a challenge to existing methods of detection due to their unique properties as their own state of matter. Liquids deform to fill their container, leading to disparate shapes of all sizes, from a mug to a lake. The same type of liquid may come in different colors, i.e. juice made from oranges versus cranberries. Its most problematic traits however lie in its optical properties: some liquids reflect their foreground like a mirror, while others are transparent like glass, resulting in arbitrary objects and scenes appearing in target regions. These characteristics make liquids fun-



Figure 1. Examples of liquids in real-world settings. The images illustrate the wide variation in appearance, color, and shape across different liquid types such as coffee, water, chemical, and juice. These examples highlight the challenges of liquid segmentation: liquids can reflect their surroundings, exhibit transparency, and deform freely to fit containers of any geometry. Such variability makes distinguishing liquid regions and classes difficult for standard segmentation methods trained on rigid and opaque objects.

damently different from the objects in common datasets which state-of-the-art methods are well suited to seeing.

There are very few existing datasets targeting the detection of general liquids, and they all come with significant drawbacks. For instance, while the UW Liquid Pouring Dataset [13] consists of 4.5 million images, they were generated purely through 3D rendering from 81 simulations, resulting in very limited variety and realism. While WaterDataset [9] and LabLiquidVolume [14] are composed of 2.3K and 5.4K real images respectively, they only consist of a singular type of liquid, water or chemicals. LabLiquidVolume additionally suffers from the inclusion of multiple camera angles of the same object while being limited to 12

predefined containers and only three colors of chemicals. Liquids outside of the laboratory setting are much more versatile in shape and appearance, varying on a sufficient level to require the consideration of separate categories, or classes, during segmentation.

To enable the proper segmentation of liquids in daily life, we introduce what is to the best of our knowledge the first dataset for the segmentation of general liquids, a **Liquid Dataset** that we call LQDS, which consists of 5K real-world images with liquids categorized into 14 classes. We evaluate state-of-the-art segmentation methods on our testing dataset and find that they struggle to handle the unusual properties of liquids, highlighting the necessity of approaching the liquid segmentation task using special methods to address these challenges.

We propose such a method, a **Liquid Detection Model** which we name LQDM, based on the observation that the liquid boundaries often exhibit higher levels of discontinuity in semantics and low-level features. LQDM’s novel architecture leverages cross-attention between two separate branches that focus on the mask and the boundary, allowing the mask branch to attend to features learned by the boundary branch. By effectively capturing these boundary features, our method is able to outperform existing methods, establishing the benchmark for the liquid segmentation task.

To summarize, our contributions are:

- We introduce the first large-scale liquid segmentation dataset LQDS, consisting of liquids in diverse scenes from the real world with corresponding masks that were manually annotated and classified.
- We propose a novel network LQDM, which uses cross attention to incorporate boundary features, enabling boundary-guided enhancement of the segmentation mask.
- We experimentally validate the effectiveness of LQDM, attaining higher accuracy on the test set of LQDS compared to state-of-the-art methods, setting the benchmark and inviting further research on the task.

2. Related Work

In this section, we survey state-of-the-art works relevant to ours, including semantic segmentation, water/chemical segmentation, and transparent/reflective object segmentation.

Semantic segmentation. The goal of semantic segmentation is to divide an image into different pixel-level segments by their class such that each pixel is assigned a class label, and the same label is assigned to separate objects. Traditionally, the task was approached using CNNs, beginning with fully convolutional networks (FCNs) [11]. FCNs treated the task as per-pixel classification, where each pixel in the input image is independently assigned a semantic label. Architectures such as DeepLab [1] built on top of the FCN and expanded the receptive field while PSPNet [22] proposed a

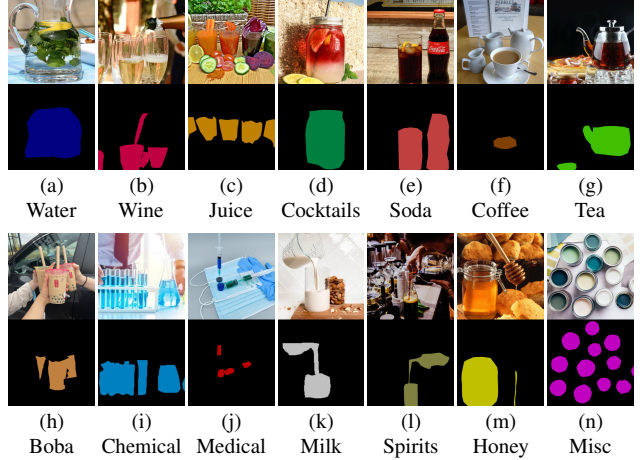


Figure 2. Examples of pairs of images and masks for each of the 14 classes in the LQDS dataset, demonstrating the variety of forms and appearances that liquids come in.

pyramid pooling module. Both these models showed that aggregating long-range context significantly improved segmentation performance at multiple scales. Following this through-line, networks such as APCNet [5] and CCNet [6] sought to capture the global context of an image, through adaptive pyramids and attention mechanisms respectively. Recently, the adoption of the vision transformer to capture image-level context enabled the removal of inductive priors toward locality inherent to CNN-based methods. The Mask Transformer framework [4] extended this further by moving away from the per-pixel classification strategy, instead introducing mask queries that learn to represent a particular segment, achieving state-of-the-art performance.

These existing methods struggle with detecting liquids, however, because liquids defy many assumptions made by top-performing segmentation models. These models are optimized to detect opaque, rigid objects that are consistent in texture and shape, relying on backbones pretrained on equally simple datasets that primarily feature solid, static objects. In this work, we address these limitations by introducing a dataset and model specifically designed to capture the unique and dynamic properties of liquids, enabling robust segmentation in real-world scenarios.

Water/chemical segmentation. Out of all the liquids, water has been the target of most works. Liang et al. in [9] construct a WaterDataset of natural water bodies like rivers and ponds to tackle the segmentation task using FCNs. However, their reliance on inductive bias through prior assumptions about the appearance of water in the dataset hinders the network’s ability to generalize to other liquids. More recently, Joo et al. in [7] achieved state-of-the-art in the water segmentation task building off a pretrained SegFormer [19], showing that vision transformers can learn the inductive bias

inherent to CNNs with sufficiently big datasets. Besides water, chemicals have been the subject of study by Schober et al. in [14], who construct a chemical dataset LabLiquidVolume and use a two-step CNN to predict chemical volume and depth. While their method excels in controlled laboratory environments, it is similarly constrained by inductive bias toward a single liquid type.

These existing works optimize for one specific liquid type by approaching it as a binary classification problem, addressing only a part of the full liquid segmentation task. By narrowing the scope, the challenge is drastically reduced, as it allows models to rely on assumptions about the uniformity in appearance, behavior, and environmental context found in a single liquid type. To our knowledge, there is no existing work targeting the semantic segmentation of general liquids, as either a binary classification task or a multi-class problem. In this work, we address this gap by introducing a comprehensive approach to liquid segmentation, treating it as a multi-class problem with 14 distinct liquid categories to capture the full diversity of real-world liquids.

Transparent/reflective object segmentation. Other objects that share the transparency or the reflectance property of liquids have also been studied in the literature. Yang et al. in [20] tackle the reflective mirror segmentation task by observing both semantic and low-level discontinuities that occur between the inside and outside of a mirror, which they extract at multiple scales using dilated convolutions in their proposed network MirrorNet. Mei et al. in [12] tackle the transparent glass segmentation similarly through observing contextual clues but at a large scale, which they extract using spatially separable convolutions with varying kernel sizes and dilation rates in their proposed network GDNet. Xie et al. tackle general transparent object segmentation, first using CNNs that integrate a boundary map in [17], and then using hybrid CNN-Transformers in [18]. Notably, Xie et al. consider the task as a multi-class problem, making the distinction between *things* and *stuff* in [17] and breaking these two categories down further in [18]. This is a step beyond MirrorNet and GDNet which treat their respective tasks as a binary classification problem similar to existing liquid segmentation methods, failing to capture the diversity of their targets.

These existing works optimize for one specific property, either transparency or reflectance. However, they are unsuitable for the segmentation of liquids because not all liquids display these properties, and those that do display these properties do so at varying degrees. For instance, while honey can be considered transparent, it applies a yellow tint to the background behind it and also distorts the image, which makes it difficult for methods such as [12, 17, 18] which expect glass-like transparency to detect it. Similarly, reflective liquids like the surface of wine and certain chemicals like gallium do not behave like a physical mirror as expected by [20], as

a result of the influence of the fresnel effect. Furthermore, because of their wide variety, different liquids may display either transparency, reflectance, or opaqueness, so using a method that considers only one of these traits is insufficient to the task as a whole. What makes it even more difficult is the fact that the same liquid may even vary between these properties. For instance, a glass of wine viewed from the side may be semi-transparent, but the same wine viewed at an oblique angle from the top may reflect surrounding objects. In this work, we aim to address these challenges by developing a holistic approach to liquid segmentation that takes into consideration the diverse and dynamic properties of liquids.

3. Liquid Segmentation Dataset

We construct the first large-scale liquid dataset, named LQDS, to address the problem of liquid segmentation. It contains 5K images of liquids, each with corresponding liquid masks that were manually annotated.

Dataset Description. LQDS contains 5000 images we manually gather, both off the internet from libraries like Open Images and Getty Images and from our surroundings using phone cameras. Consequently, our data has wide distributions in scale, perspective, and backgrounds. The liquid objects in the images are categorized into 14 classes: water, wine, juice, cocktails, soda, coffee, tea, boba, chemical, medical, milk, spirits, honey, and miscellaneous, appearing in different frequencies shown in Figure 3a. For dividing into the training set and testing set, we use a stratified split with random sampling that preserves the proportion of each class between the two sets, landing with 4200 images for training and 800 images for testing.

Annotation. For high-quality annotation, each image in our dataset is manually labeled by experts (e.g., students who work on related fields). The format of the mask image is in line with other semantic segmentation datasets such as ADE20K [23], where 0 denotes background and classes are set to values between 1-14. Most liquids are held inside a container, which we do not include as part of the mask, as seen in Figure 2. We also exclude other possible objects that appear inside the liquid, for example straws and spoons. To maintain consistency in labeling each of the liquids into the 14 categories, one of us does all the classifying at the end. To further ensure the annotation quality, we perform multiple rounds of inspection and refinement until the annotation of each image meets the requirement.

Dataset Analysis. The properties of the liquid objects in LQDS are shown in Figure 3, including object count distribution and pixel distribution per class, as well as the liquid area and location in the images.

- **Object count distribution.** Figure 3a shows, for each class, the percentage of images in which it appears at least once. There are 117 images in the training set and

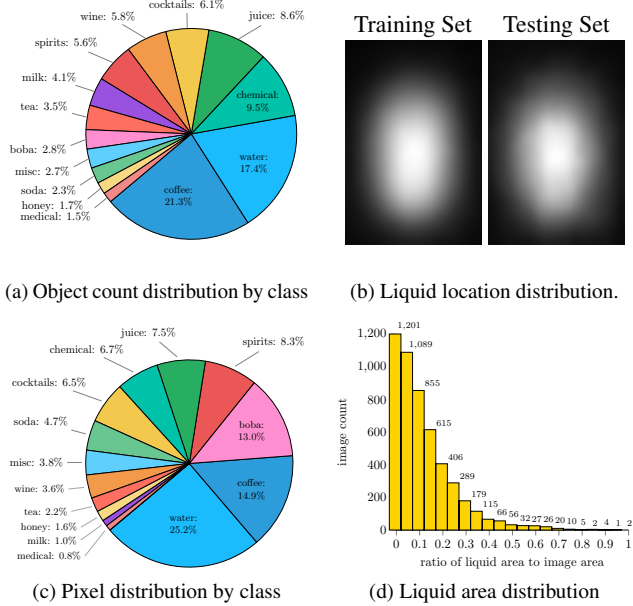


Figure 3. Statistics of the LQDS dataset.

21 images in the testing set which contain multiple classes. Coffee appears the most, followed by water, chemicals, juice, and then the alcoholic beverages. Our classes cover all liquid types that can be encountered on a regular basis, from everyday drinks like coffee and juice, to alcohol like cocktails and wine, to undrinkable chemicals and the miscellaneous.

- **Pixel distribution.** Figure 3c shows, for each class, the percentage of mask pixels it takes up in the entire dataset. Compared with the object count distribution, water takes up most of the mask pixels rather than coffee, which makes sense as water is not limited to appearing in a small cup.
- **Liquid location in image.** Liquid objects in our dataset are located at all positions throughout the image, as seen in Figure 3b, and we compute probability maps for the likelihood that a pixel is part of the liquid area. It can be seen that the liquids tend towards the center of the image since their containers are usually placed at the focus of the image, and this is consistent across both the training and testing set.
- **Liquid Area.** We calculate the percentage of the image taken up by the area of liquid in Figure 3d. It can be seen that the LQDS dataset contains liquids of varying sizes, with most falling below the 20% mark. These are the liquids most common in everyday life, appearing in cups, bottles, and glasses. Above the 20% mark consists of both larger liquid bodies, such as fish tanks and pools, as well as more close-up shots of the small objects.

4. Proposed Network

We observe that there tends to be higher levels of discontinuity in content and low-level color or texture at the boundary of liquids, and we argue that these boundaries are easier to detect due to this contrast. We take advantage of this by proposing a dual-branch architecture to inject boundary features into mask predictions through cross-attention.

4.1. Overview

Figure 4 illustrates our architecture, LQDM, consisting of two distinct output layers that facilitate multi-task learning. For a single image, feature embeddings are extracted by a vision transformer (ViT) backbone using L_1 transformer encoder blocks. Following these shared blocks, we split into two separate branches: the mask branch and the boundary branch. For each branch, we introduce a set of K learnable queries. These queries are processed by L_2 cross-attention blocks as per Section 4.2, allowing the mask branch to attend to the boundary branch. Following cross-attention, the queries are concatenated onto the feature embeddings of their respective branch, and together they are processed by L_2 transformer encoder blocks. Notably, these transformer encoder blocks are shared between the two branches, which we discover leads to better performance while being more parameter efficient and takes up less memory during training. We argue that this is because a shared structure allows the vision transformer backbone to learn the boundary features at a deeper level.

To produce the final logits for prediction, a mask module is installed to process the query and feature embedding outputs of the last transformer encoder block. The class logits are acquired using a linear layer, while the mask and boundary logits are acquired using multilayer perceptrons followed by dot products with upscaled image features.

4.2. Boundary Attention

To leverage boundary information for improved mask prediction, we introduce cross-attention blocks alongside each transformer encoder block, which allow the mask branch to attend to features from the boundary branch. Specifically, at every i -th pair of cross-attention and transformer encoder blocks, we take the two sets of K learnable queries from both the mask branch and the boundary branch and apply cross-attention between them, with the mask queries $Q_m^{(i)}$ serving as the query and the boundary queries at the same block $Q_b^{(i)}$ providing the key and value pairs:

$$Q_m^{(i)} = Q_m^{(i)} + \text{CrossAttnBlock}(Q_m^{(i)}, Q_b^{(i)}) \quad (1)$$

where CrossAttnBlock implements standard multi-head cross-attention. We normalize both Q_m and Q_b using layer normalization before producing the queries and key-value pairs from them using projection layers. The

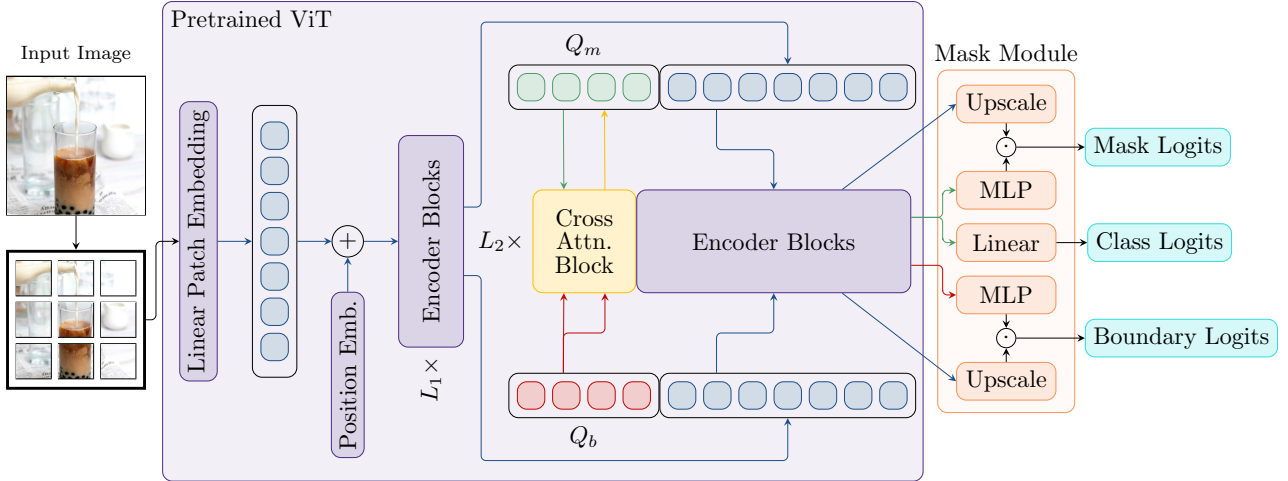


Figure 4. Overview of the proposed dual-branch architecture, LQDM. A ViT backbone first extracts shared feature embeddings through L_1 transformer encoder blocks. The network then splits into two branches: the *mask branch* for semantic segmentation and the *boundary branch* for boundary prediction. Each branch adds K learnable queries to its feature embeddings, which pass through L_2 cross-attention blocks that apply cross-attention as per Equation 1, while the combined query and feature embeddings pass through L_2 transformer encoder blocks, enabling the mask branch to attend to boundary features. The outputs of each branch are processed by the mask module which produces mask, boundary, and class logits, which are used to compute training loss as per Equation 2.

cross-attention block is applied alongside each of the L_2 transformer blocks, allowing progressive refinement of mask predictions guided by boundary features. Our cross-attention mechanism allows the network to selectively attend to relevant boundary features at different spatial locations, leading to more accurate segmentation especially along liquid edges where transparency and reflection create ambiguities.

4.3. Mask Module

We use a mask module as per [4, 8] to obtain class, mask, and boundary logits. The mask module takes as inputs the corresponding queries and image feature embeddings of the mask and boundary branch following the last of the L_2 cross-attention and transformer encoder blocks. For the class logits, the queries are passed through a simple linear layer. For the mask and boundary logits, the respective queries are passed first through a three-layer MLP, and the logits are then produced from a dot product with the upscaled image feature embeddings.

4.4. Loss Function

The segmentation and boundary logits obtained from the mask module are used to compute overall training loss. In order to supervise both branches during training, we define the total loss as the weighted sum of the mask branch loss and the boundary branch loss:

$$L = L_m + \omega L_b \quad (2)$$

where L_m and L_b denote the mask and boundary losses,

balanced by the parameter ω . We empirically set ω to 200 in our experiments. For calculating L_b , we use the standard binary cross-entropy (BCE) loss. We calculate boundary BCE loss using boundary ground-truths generated as a binary mask with a thickness of 1% of the image diagonal length (computed as $\sqrt{H^2 + W^2}$).

5. Experiments

5.1. Implementation Details

We implement LQDM using the PyTorch framework. For training, we use a 512×512 input size into the model, augmented using a sequence of color jittering, random horizontal flipping, scale jittering, padding, and random cropping. For the feature extraction backbone, we choose a pretrained SigLIP-SO400M [16], and use $L_1 = 20$, $L_2 = 4$. The other parts of our network are initialized randomly. For the multi-head cross-attention operation, we use 8 attention heads with a dropout rate of 0.2. For loss optimization, we use the AdamW optimizer with a learning rate of 0.0001 and layer-wise learning rate decay of 0.8 for 16 epochs. We train on four NVIDIA A5500 GPUs with a batch size of four per GPU. On this hardware, it takes about six hours for the network to converge. For inference, the shorter side of the image is resized to the input size 512, and the model processes the image in squares using a sliding-window fashion along the longer side.

Evaluation metrics. For a comprehensive evaluation, we adopt the Intersection over Union (IoU) and pixel accuracy

Table 1. Per-class IoU performance on the testing set of LQDS for evaluated state-of-the-art segmentation methods, sorted by mean IoU. Our proposed method LQDM achieves the highest mean IoU and additionally outperforms the other methods in a majority (11/14) of the individual class IoUs.

| Model | water | wine | juice | cocktails | soda | coffee | tea | boba | chemical | medical | milk | spirits | honey | misc | mIoU \uparrow |
|-------------|--------------|--------------|--------------|--------------|--------------|--------------|--------------|--------------|--------------|--------------|--------------|--------------|--------------|--------------|-----------------|
| Knet | 21.01 | 10.87 | 28.94 | 8.45 | 13.09 | 39.97 | 2.93 | 56.42 | 15.80 | 0.74 | 1.08 | 20.04 | 17.54 | 23.27 | 18.58 |
| TransLab | 35.94 | 11.63 | 42.73 | 2.84 | 15.50 | 40.52 | 0.12 | 49.13 | 25.78 | 0.00 | 38.63 | 28.08 | 21.52 | 4.20 | 22.62 |
| GCNet | 28.80 | 13.11 | 33.88 | 39.78 | 11.63 | 47.11 | 10.26 | 46.49 | 16.53 | 0.00 | 23.53 | 33.35 | 15.73 | 32.37 | 25.18 |
| ANN | 59.40 | 14.92 | 44.85 | 33.79 | 53.83 | 59.10 | 14.37 | 63.86 | 43.63 | 19.13 | 39.26 | 46.13 | 63.97 | 33.44 | 42.12 |
| Segmenter | 54.14 | 16.36 | 48.22 | 44.92 | 42.91 | 63.55 | 15.94 | 62.93 | 37.90 | 24.66 | 50.94 | 50.50 | 51.51 | 37.25 | 42.98 |
| FCN | 44.10 | 16.46 | 48.63 | 45.42 | 52.38 | 61.45 | 13.65 | 62.88 | 42.07 | 23.30 | 52.31 | 40.27 | 62.68 | 37.11 | 43.05 |
| PSPNet | 50.54 | 21.12 | 48.47 | 43.37 | 56.45 | 59.89 | 13.88 | 61.38 | 44.69 | 13.21 | 50.87 | 44.91 | 60.42 | 42.51 | 43.69 |
| APCNet | 54.06 | 20.66 | 50.98 | 40.94 | 52.01 | 63.70 | 16.57 | 65.11 | 39.38 | 13.48 | 62.98 | 32.91 | 66.84 | 34.83 | 43.89 |
| DeepLabV3+ | 53.39 | 16.25 | 50.77 | 34.62 | 48.93 | 61.22 | 12.91 | 68.33 | 45.70 | 24.43 | 48.78 | 46.90 | 65.78 | 39.16 | 44.08 |
| Mask2Former | 49.36 | 15.18 | 50.02 | 39.24 | 45.77 | 60.67 | 8.93 | 65.81 | 30.35 | 22.03 | 60.86 | 51.64 | 70.81 | 46.66 | 44.10 |
| CCNet | 48.67 | 15.35 | 49.74 | 47.06 | 56.85 | 62.53 | 21.71 | 66.07 | 45.92 | 25.56 | 47.42 | 46.04 | 59.94 | 35.21 | 44.86 |
| Maskformer | 43.24 | 18.11 | 50.16 | 45.10 | 60.61 | 62.22 | 16.99 | 70.87 | 42.47 | 18.38 | 59.66 | 48.75 | 56.58 | 37.52 | 45.05 |
| Segformer | 54.94 | 19.09 | 48.34 | 42.11 | 62.95 | 65.19 | 9.83 | 74.24 | 35.22 | 24.88 | 46.29 | 52.77 | 64.56 | 36.20 | 45.47 |
| Swin | 40.76 | 15.21 | 51.54 | 43.47 | 56.34 | 66.13 | 12.78 | 76.11 | 39.67 | 31.37 | 67.19 | 46.67 | 60.15 | 34.73 | 45.87 |
| EoMT | 72.25 | 18.77 | 44.65 | 34.69 | 74.22 | 68.91 | 21.52 | 77.40 | 53.98 | 29.84 | 44.44 | 60.86 | 53.71 | 46.45 | 50.12 |
| LQDM | 75.68 | 35.97 | 56.41 | 44.00 | 79.63 | 74.55 | 16.09 | 78.63 | 55.04 | 59.36 | 68.50 | 63.23 | 78.93 | 43.87 | 59.28 |

Table 2. Per-class pixel-accuracy (PA) performance on the testing set of LQDS for evaluated state-of-the-art segmentation methods, sorted by mean PA. Our proposed method LQDM achieves the highest mean PA and additionally outperforms the other methods in most (8/14) of the individual class PA. Note that the TransLab codes only provide the overall PA.

| Model | water | wine | juice | cocktails | soda | coffee | tea | boba | chemical | medical | milk | spirits | honey | misc | mPA \uparrow |
|-------------|--------------|--------------|--------------|--------------|--------------|--------------|--------------|--------------|--------------|--------------|--------------|--------------|--------------|--------------|----------------|
| TransLab | - | - | - | - | - | - | - | - | - | - | - | - | - | - | 38.25 |
| GCNet | 31.14 | 15.09 | 49.85 | 50.31 | 88.45 | 71.11 | 19.72 | 74.89 | 34.57 | 0.00 | 48.80 | 55.56 | 57.59 | 43.98 | 45.79 |
| Knet | 34.47 | 26.58 | 50.00 | 26.91 | 64.68 | 57.68 | 15.06 | 71.62 | 52.33 | 23.49 | 22.17 | 65.60 | 82.77 | 49.94 | 45.95 |
| ANN | 65.84 | 16.71 | 63.07 | 43.74 | 66.59 | 79.67 | 16.74 | 76.77 | 53.66 | 22.25 | 51.59 | 71.48 | 77.98 | 39.75 | 53.27 |
| Segmenter | 61.85 | 17.86 | 62.49 | 57.53 | 52.64 | 81.92 | 17.06 | 71.18 | 52.16 | 27.99 | 57.29 | 76.04 | 72.40 | 39.73 | 53.44 |
| FCN | 52.32 | 18.65 | 68.61 | 54.60 | 61.91 | 81.75 | 17.86 | 73.67 | 52.03 | 26.94 | 56.57 | 60.79 | 80.21 | 42.75 | 53.48 |
| Mask2Former | 59.15 | 16.83 | 66.87 | 53.02 | 48.98 | 72.17 | 12.67 | 72.03 | 45.90 | 28.49 | 75.97 | 80.31 | 78.87 | 49.68 | 54.35 |
| APCNet | 64.42 | 22.86 | 67.71 | 50.32 | 66.26 | 84.64 | 18.07 | 76.02 | 50.17 | 23.33 | 66.68 | 54.04 | 81.86 | 42.38 | 54.91 |
| DeepLabV3+ | 60.47 | 18.29 | 69.90 | 42.74 | 61.55 | 76.99 | 16.53 | 84.59 | 55.14 | 27.49 | 59.69 | 72.88 | 81.80 | 43.50 | 55.11 |
| PSPNet | 56.24 | 23.48 | 70.05 | 53.94 | 64.94 | 80.33 | 18.48 | 72.46 | 53.34 | 22.78 | 63.35 | 70.31 | 76.74 | 45.89 | 55.17 |
| Maskformer | 50.08 | 20.76 | 66.41 | 55.90 | 68.37 | 77.26 | 21.48 | 79.73 | 62.34 | 28.08 | 63.45 | 81.00 | 65.73 | 42.54 | 55.94 |
| CCNet | 54.44 | 17.50 | 66.49 | 56.92 | 70.36 | 79.69 | 25.44 | 79.56 | 56.01 | 30.25 | 56.63 | 73.15 | 80.98 | 38.29 | 56.12 |
| Swin | 45.47 | 17.17 | 64.99 | 54.05 | 69.95 | 80.20 | 15.72 | 87.12 | 53.99 | 37.72 | 70.20 | 74.66 | 80.65 | 36.25 | 56.30 |
| Segformer | 62.64 | 21.59 | 62.27 | 55.97 | 73.56 | 82.76 | 10.87 | 88.52 | 53.41 | 26.50 | 64.14 | 76.65 | 76.89 | 42.45 | 57.02 |
| EoMT | 82.09 | 21.60 | 59.61 | 51.84 | 85.23 | 89.06 | 24.50 | 87.79 | 78.37 | 39.08 | 76.02 | 83.13 | 87.83 | 54.85 | 65.79 |
| LQDM | 83.18 | 44.58 | 72.98 | 56.11 | 88.43 | 86.34 | 17.08 | 92.05 | 67.66 | 80.94 | 75.06 | 83.42 | 91.69 | 62.99 | 71.61 |

(PA) metrics standard for image segmentation. For both the mean IoU and mean PA, we only factor in the values from the object classes, ignoring background.

5.2. Comparison with State-of-the-Arts

For our evaluation, we select 15 state-of-the-art methods in semantic segmentation, including both well-established CNN-based models such as DeepLabV3+ [2], PSPNet [22], APCNet [5], FCN [11], ANN [24], TransLab [17], KNet [21], and CCNet [6] and more recent transformer-based models such as Swin [10], MaskFormer [3], Mask2Former [4], Segmenter [15], Segformer [19], GCNet [6], and EoMT [8]. For a fair comparison, we retrain each of these networks on the training set of LQDS using

their publicly available implementations and parameter settings, and evaluate them on the LQDS testing set.

Table 1 reports the per-class liquid segmentation performance on the testing set of LQDS for the IoU metric, and Table 2 reports the per-class pixel-accuracy metrics. Our method outperforms all others in both metrics, with 59.28% mean IoU and 71.61% mean pixel-accuracy.

Figure 5 shows visual comparisons of segmentation produced by our method and the evaluated state-of-the-arts. It can be seen that our method is especially effective on the images where the foreground or background are semantically complex and many objects are intersecting with the target region, such as in rows 1 and 2. Our method is able to iden-

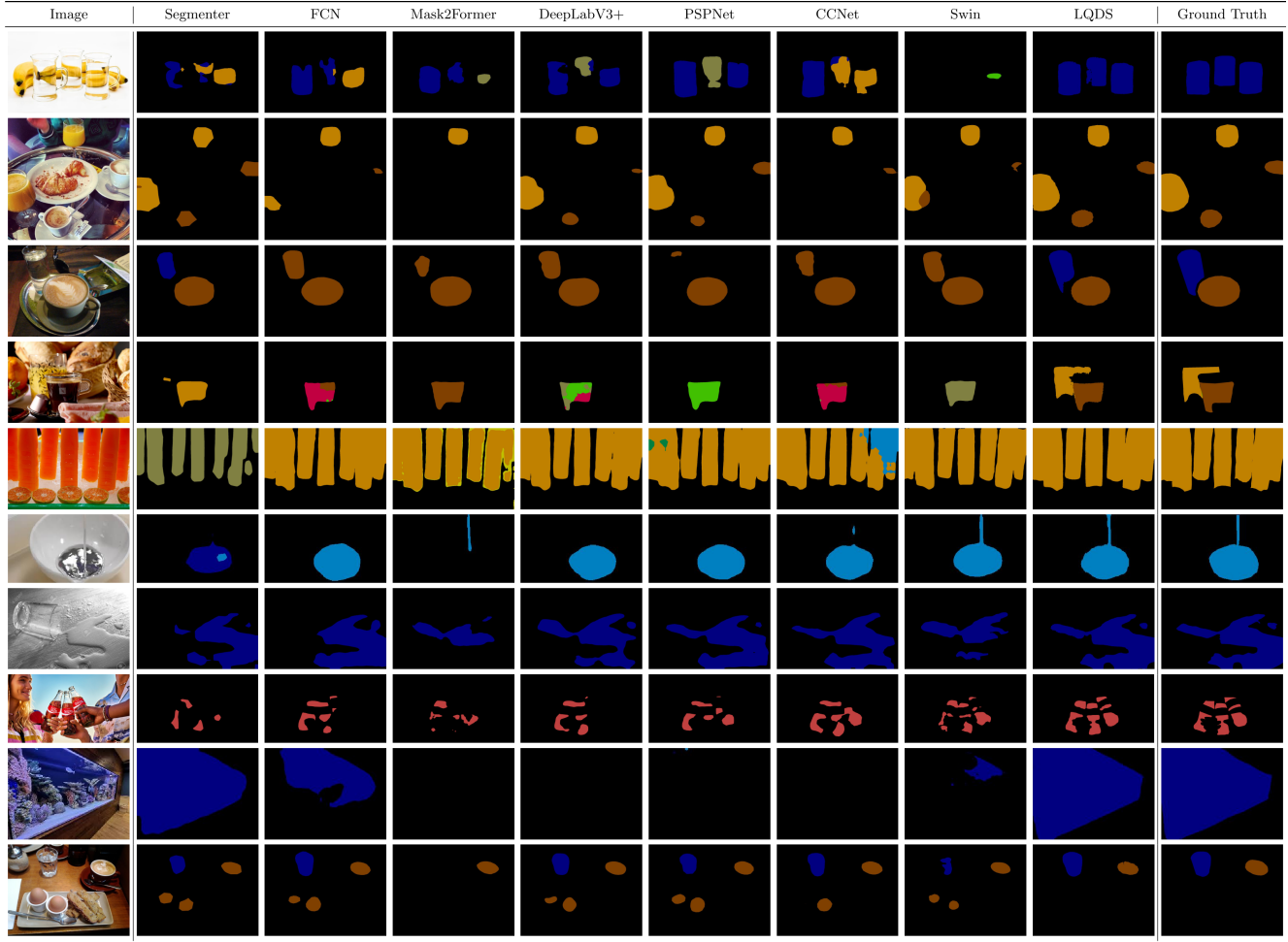


Figure 5. Visual comparison of LQDM to other semantic segmentation methods on images from the LQDS testing set.

Table 3. Performance on easy and hard subsets of the testing set.

| Method | Easy IoU | Hard IoU | Easy Acc | Hard Acc |
|--------|----------|----------|----------|----------|
| EoMT | 51.08 | 45.41 | 65.41 | 64.32 |
| LQDS | 62.03 | 53.12 | 73.12 | 66.84 |

tify the liquids where others fail to see it completely, such as in row 9, but it is also less prone to false positives, such as in row 10. Additionally, our method is able to correctly classify the liquids where others mistake it for another class, such as in rows 3 and 4.

We further provide a split of the testing set into hard and easy subsets, with 353 hard images and 447 easy images. We define easy as images limited to a single object or a single class with a regular shape that stands out in the foreground. Liquids in the hard set are more crowded and occluded and display more of their unique liquid properties, such as deforming while being poured and reflecting the surroundings.

Table 4. Component analysis. BL is the baseline, SL is the SigLIP weights, BB is the boundary branch, BCA is the boundary cross attention between the boundary branch and the mask branch.

| Components | mIoU | mAcc | mPrec | mF1 |
|--------------|--------------|--------------|--------------|--------------|
| BL | 50.12 | 65.79 | 67.46 | 63.15 |
| BL+SL | 56.50 | 70.28 | 72.41 | 69.03 |
| BL+SL+BB | 57.91 | 71.30 | 74.69 | 70.57 |
| BL+SL+BB+BCA | 59.28 | 71.61 | 76.63 | 71.50 |

Table 3 shows the performance difference of our baseline and our proposed method between the two sets.

5.3. Component Analysis

Architecture components. Table 4 evaluates the effectiveness of our proposed method. For this part, in addition to the IoU and PA metrics, we calculate the pixel pre-



Figure 6. Visualization of predicted boundaries by LQDM.

Table 5. Performance for different values of the parameter ω .

| ω | mIoU | mAcc | mPrec | mF1 |
|----------|-------|-------|-------|-------|
| 1.0 | 54.56 | 68.06 | 70.61 | 66.79 |
| 10.0 | 56.01 | 69.50 | 73.98 | 68.17 |
| 100.0 | 54.88 | 67.80 | 72.18 | 66.86 |
| 200.0 | 59.28 | 71.61 | 76.63 | 71.50 |

cision and F1 score. The F1 score is a combination of both the recall and precision metrics, and is calculated as $F1 = 2 \cdot \frac{precision \cdot recall}{precision + recall}$. For our baseline, we use EoMT, pretrained with a DINOv2 backbone as per the original implementation. Through experimentation we find that initializing the model with weights from the more recent SigLIP2 encoder provides significantly better performance for our following tasks. We then show that the performance of mask segmentation already improves by just using the boundary branch as an auxiliary task, demonstrating the necessity of factoring in the boundary when segmenting liquids. Finally, we show that incorporating cross-attention between the mask branch and the boundary branch further enhances segmentation performance by enabling the mask branch to integrate boundary features effectively. With this, our full network is able to attain the highest performance on all four metrics.

Impact of parameter ω . We use this parameter in Equation 2 to balance the loss between the mask branch and the boundary branch. Different values of ω are tested in Table 5. We find that values beyond 200 is when additional performance benefits level out.

5.4. Segmentation Outside of Liquids

We discover that our boundary-enhanced model provides improved performance for objects outside of liquids as well. For testing this, we use the ADE20K [23] dataset, which is the standard semantic segmentation benchmark. ADE20K consists of 20K images with 150 classes. Table 6 displays the results of our model, and it can be seen that our model



(a) False negative. In this image, the layer of water is so thin that there is no contrast in the boundary area where the water begins and ends, and as a result our model fails to detect any liquid there.

(b) Misclassification. In this image, our model correctly segments the left and right liquids as water and wine, but the tinted cup in the middle leads our model to detect its contents as wine.

Figure 7. Failure case analysis.

Table 6. Performance of LQDM in general object segmentation on the ADE20K benchmark.

| Method | Params | GFLOPs | mIoU |
|-------------|--------|--------|------|
| Mask2Former | 351M | 910 | 58.9 |
| EoMT-DinoV2 | 319M | 721 | 58.4 |
| EoMT-DinoV3 | 319M | 721 | 59.5 |
| LQDS | 453M | 934 | 59.6 |

generalizes well to less challenging objects, achieving a mean IoU of 59.6%.

6. Conclusion

In this work, we aim to address the challenging problem of segmenting liquids in real-world images. We present LQDS, the first large-scale dataset for general liquid segmentation, containing 5,000 manually annotated images across 14 distinct liquid classes. Unlike previous datasets limited to single liquid types or synthetic data, LQDS captures the diverse appearances, shapes, and optical properties of liquids encountered in daily life, from transparent and reflective surfaces to various colors and containers. To tackle the unique challenges posed by liquid segmentation, we proposed LQDM, a novel dual-branch architecture that leverages boundary information through cross-attention mechanisms. By allowing the mask branch to attend to features from a dedicated boundary branch, our method effectively handles the ambiguities created by transparency and reflection at liquid edges. Extensive experiments demonstrate that LQDM outperforms state-of-the-art semantic segmentation methods on the LQDS test set, establishing a strong baseline for this task that we show remains largely unsolved. We believe that LQDS and LQDM will facilitate future research in liquid segmentation and enable practical applications in robotics, where the ability to detect and avoid liquids is crucial for safe navigation and manipulation.

References

- [1] Liang-Chieh Chen, George Papandreou, Iasonas Kokkinos, Kevin Murphy, and Alan L. Yuille. Deeplab: Semantic image segmentation with deep convolutional nets, atrous convolution, and fully connected crfs. *CoRR*, abs/1606.00915, 2016. 2
- [2] Liang-Chieh Chen, Yukun Zhu, George Papandreou, Florian Schroff, and Hartwig Adam. Encoder-decoder with atrous separable convolution for semantic image segmentation. In *Proceedings of the European Conference on Computer Vision (ECCV)*, 2018. 6
- [3] Bowen Cheng, Alex Schwing, and Alexander Kirillov. Per-pixel classification is not all you need for semantic segmentation. In *Advances in Neural Information Processing Systems*, pages 17864–17875. Curran Associates, Inc., 2021. 6
- [4] Bowen Cheng, Ishan Misra, Alexander G. Schwing, Alexander Kirillov, and Rohit Girdhar. Masked-attention mask transformer for universal image segmentation. In *Proceedings of the IEEE/CVF Conference on Computer Vision and Pattern Recognition (CVPR)*, 2022. 2, 5, 6
- [5] Junjun He, Zhongying Deng, Lei Zhou, Yali Wang, and Yu Qiao. Adaptive pyramid context network for semantic segmentation. In *Proceedings of the IEEE/CVF Conference on Computer Vision and Pattern Recognition (CVPR)*, 2019. 2, 6
- [6] Zilong Huang, Xinggang Wang, Lichao Huang, Chang Huang, Yunchao Wei, and Wenyu Liu. Ccnet: Criss-cross attention for semantic segmentation. In *Proceedings of the IEEE/CVF International Conference on Computer Vision (ICCV)*, 2019. 2, 6
- [7] Hanseon Joo, Eunji Lee, and Minjong Cheon. Habaek: High-performance water segmentation through dataset expansion and inductive bias optimization, 2024. 2
- [8] Tommie Kerssies, Niccolò Cavagnero, Alexander Hermans, Narges Norouzi, Giuseppe Averta, Bastian Leibe, Gijs Dubbelman, and Daan de Geus. Your ViT is Secretly an Image Segmentation Model. In *Proceedings of the IEEE/CVF Conference on Computer Vision and Pattern Recognition (CVPR)*, 2025. 5, 6
- [9] Yongqing Liang, Navid Jafari, Xing Luo, Qin Chen, Yanpeng Cao, and Xin Li. Waternet: An adaptive matching pipeline for segmenting water with volatile appearance. *Computational Visual Media*, 6(1):65–78, 2020. 1, 2
- [10] Ze Liu, Yutong Lin, Yue Cao, Han Hu, Yixuan Wei, Zheng Zhang, Stephen Lin, and Baining Guo. Swin transformer: Hierarchical vision transformer using shifted windows. In *Proceedings of the IEEE/CVF International Conference on Computer Vision (ICCV)*, 2021. 6
- [11] Jonathan Long, Evan Shelhamer, and Trevor Darrell. Fully convolutional networks for semantic segmentation. In *Proceedings of the IEEE Conference on Computer Vision and Pattern Recognition (CVPR)*, 2015. 2, 6
- [12] Haiyang Mei, Xin Yang, Yang Wang, Yuanyuan Liu, Shengfeng He, Qiang Zhang, Xiaopeng Wei, and Rynson W.H. Lau. Don't hit me! glass detection in real-world scenes. In *Proceedings of the IEEE/CVF Conference on Computer Vision and Pattern Recognition (CVPR)*, 2020. 3
- [13] Connor Schenck and Dieter Fox. Perceiving and reasoning about liquids using fully convolutional networks. *Int. J. Robotics Res.*, 37(4-5):452–471, 2017. 1
- [14] Daniel Schober, Ronja Güldenring, James Love, and Lazaros Nalpantidis. Vision-based robot manipulation of transparent liquid containers in a laboratory setting, 2024. 1, 3
- [15] Robin Strudel, Ricardo Garcia, Ivan Laptev, and Cordelia Schmid. Segmenter: Transformer for semantic segmentation. In *Proceedings of the IEEE/CVF International Conference on Computer Vision (ICCV)*, 2021. 6
- [16] Michael Tschannen, Alexey Gritsenko, Xiao Wang, Muhammad Ferjad Naeem, Ibrahim Alabdulmohsin, Nikhil Parthasarathy, Talfan Evans, Lucas Beyer, Ye Xia, Basil Mustafa, Olivier H'enaff, Jeremiah Harmsen, Andreas Steiner, and Xiaohua Zhai. Siglip 2: Multilingual vision-language encoders with improved semantic understanding, localization, and dense features. *arXiv preprint arXiv:2502.14786*, 2025. 5
- [17] Enze Xie, Wenjia Wang, Wenhui Wang, Mingyu Ding, Chunhua Shen, and Ping Luo. Segmenting transparent objects in the wild. In *Proceedings of the European Conference on Computer Vision (ECCV)*, 2020. 3, 6
- [18] Enze Xie, Wenjia Wang, Wenhui Wang, Peize Sun, Hang Xu, Ding Liang, and Ping Luo. Segmenting transparent object in the wild with transformer. In *Proceedings of the Thirty-Second International Joint Conference on Artificial Intelligence, IJCAI-23*. International Joint Conferences on Artificial Intelligence Organization, 2021. 3
- [19] Enze Xie, Wenhui Wang, Zhiding Yu, Anima Anandkumar, Jose M. Alvarez, and Ping Luo. Segformer: Simple and efficient design for semantic segmentation with transformers. In *Advances in Neural Information Processing Systems*, pages 12077–12090. Curran Associates, Inc., 2021. 2, 6
- [20] Xin Yang, Haiyang Mei, Ke Xu, Xiaopeng Wei, Baocai Yin, and Rynson W.H. Lau. Where is my mirror? In *Proceedings of the IEEE/CVF International Conference on Computer Vision (ICCV)*, 2019. 3
- [21] Wenwei Zhang, Jiangmiao Pang, Kai Chen, and Chen Change Loy. K-net: Towards unified image segmentation. In *Advances in Neural Information Processing Systems*, pages 10326–10338. Curran Associates, Inc., 2021. 6
- [22] Hengshuang Zhao, Jianping Shi, Xiaojuan Qi, Xiaogang Wang, and Jiaya Jia. Pyramid scene parsing network. In *Proceedings of the IEEE Conference on Computer Vision and Pattern Recognition (CVPR)*, 2017. 2, 6
- [23] Bolei Zhou, Hang Zhao, Xavier Puig, Sanja Fidler, Adela Barriuso, and Antonio Torralba. Scene parsing through ade20k dataset. In *Proceedings of the IEEE Conference on Computer Vision and Pattern Recognition (CVPR)*, 2017. 3, 8
- [24] Zhen Zhu, Mengde Xu, Song Bai, Tengteng Huang, and Xiang Bai. Asymmetric non-local neural networks for semantic segmentation. In *Proceedings of the IEEE/CVF International Conference on Computer Vision (ICCV)*, 2019. 6